AD-A074 163 WASHINGTON UNIV SEATTLE DEPT OF CHEMISTRY F/G 7/3
COLLISIONAL RELAXATION OF TRANSIENT VIBRATIONAL ENERGY DISTRIBU--ETC(U)
SEP 79 D F KELLEY, L ZALOTAI, B S RABINOVITCH N00014-75-C-0690
UNCLASSIFIED TR-011 NL

| OF |
ADA
074163

END
DATE FILMED
10-79
DDC

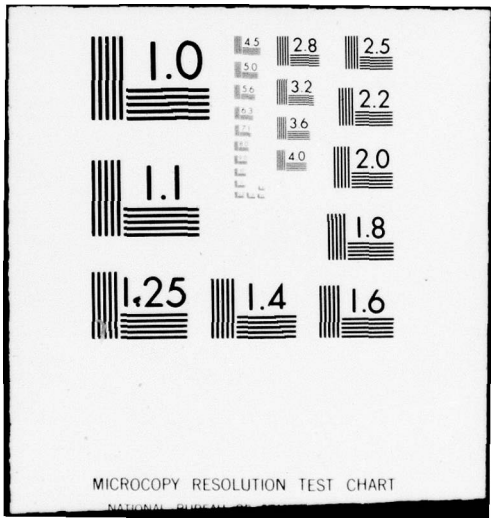
1.0
1.1
1.25
1.4
1.6
1.8
2.0
2.2
2.5
2.8
3.2
3.6
4.0
4.5
5.0
5.6
6.3
MICROCOPY RESOLUTION TEST CHART

Collisional Relaxation of Transient Vibrational Energy Distributions in a Thermal Unimolecular System. The Variable Encounter Method.

(10) D. F. Kelley, L. Zalotai and B. S. Rabinovitch

Department of Chemistry, BG-10
University of Washington
Seattle, WA 98195

Prepared for Publication in Chemical Physics

(9) Technical Report No. NR092-549-~~TR11~~ TR011

Contract N00014-75-C-0690, NR092-549

(13)

(11) 15 September 15, 1979

(12) 42p.

(14) TR-011

OFFICE OF NAVAL RESEARCH
Department of the Navy
Code 473
800 N. Quincy
Arlington, VA 2217

Unclassified

SECURITY CLASSIFICATION OF THIS PAGE (When Data Entered)

REPORT DOCUMENTATION PAGE		READ INSTRUCTIONS BEFORE COMPLETING FORM
1. REPORT NUMBER NR092-549-TR011	2. GOVT ACCESSION NO.	3. RECIPIENT'S CATALOG NUMBER
4. TITLE (and Subtitle) Collisional Relaxation of Transient Vibrational Energy Distributions in a Thermal Unimolecular System. The Variable Encounter Method		5. TYPE OF REPORT & PERIOD COVERED Technical 6. PERFORMING ORG. REPORT NUMBER
7. AUTHOR(s) D. F. Kelley, L. Zalotai and B. S. Rabinovitch		8. CONTRACT OR GRANT NUMBER(s) N00014-75-C-0690 NR 092-549
9. PERFORMING ORGANIZATION NAME AND ADDRESS Professor B. S. Rabinovitch Department of Chemistry BG-10 University of Washington Seattle, WA 98195		10. PROGRAM ELEMENT, PROJECT, TASK AREA & WORK UNIT NUMBERS
11. CONTROLLING OFFICE NAME AND ADDRESS Office of Naval Research, Code 743 Department of the Navy 800 N. Quincy Arlington, VA 22217		12. REPORT DATE 15 Sept. 79 13. NUMBER OF PAGES 36
14. MONITORING AGENCY NAME & ADDRESS(if different from Controlling Office)		15. SECURITY CLASS. (of this report) Unclassified 15a. DECLASSIFICATION/DOWNGRADING SCHEDULE

16. DISTRIBUTION STATEMENT (of this Report)

This document has been approved for public release; its distribution is unlimited.

17. DISTRIBUTION STATEMENT (of the abstract entered in Block 20, if different from Report)

18. SUPPLEMENTARY NOTES

Submitted to Chemical Physics

19. KEY WORDS (Continue on reverse side if necessary and identify by block number)

Cyclopropane
Energy Transfer
High Temperatures
Surface
Transients
Unimolecular Reaction
Variable Encounter Method
Vibrational Relaxation

20. ABSTRACT (Continue on reverse side if necessary and identify by block number)

The Variable Encounter Method is described in detail together with theoretical models for deconvolution of data. A relation is developed between mean first passage time and "incubation" time. Application is made to the study of the transient region in vibrational accommodation of cyclopropane-d_2 at high temperature surfaces. Collision efficiency declines with rise of temperature. Surface collisions are more efficient than binary gas phase encounters.

DD FORM 1 JAN 73 1473 EDITION OF 1 NOV 65 IS OBSOLETE
S/N 0102-LF-014-6601

SECURITY CLASSIFICATION OF THIS PAGE (When Data Entered)

DISTRIBUTION LIST

Contractor University of Washington NR 092-549

Contract Number N00014-75-C-0690 Date September 15, 1979

	No. Copies
Office of Naval Research Code 473 Arlington, VA 22217 Attn: Dr. Richard Miller	10
Office of Naval Research Branch Office 1030 East Green Street Pasadena, CA 91106 Attn: Dr. R. J. Marcus	1
Office of Naval Research Branch Office 536 S. Clark Street Chicago, IL 60605 Attn: Dr. J. Smith	1
Defense Documentation Center Bldg. 5 Cameron Station Alexandria, VA 22314	12
Office of Naval Research Branch Office 495 Summer Street Boston, MA 02210 Attn: Dr. L. H. Peebles	1
Office of Naval Research Resident Representative University of Washington 1107 N.E. 45, Univ. Dist. Bldg., Rm 422 Seattle, WA 98195	1
U. S. Naval Research Laboratory Code 2627 Washington, D.C. 20375	6
Naval Research Laboratory Code 6100 Washington, D.C. 20375	1
Naval Air Systems Command Code 440 Washington, D.C. 20360 Attn: Dr. H. Rosenwasser	1

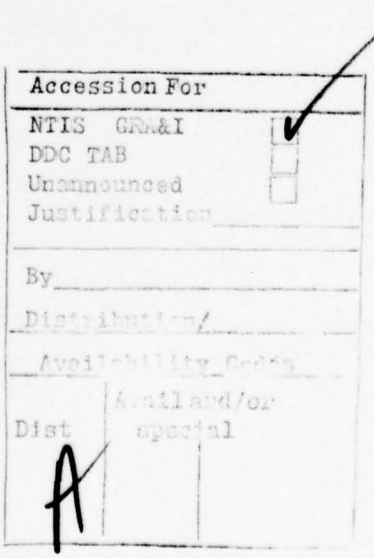

	No. Copies
Naval Sea Systems Command SEA-0331 Washington, D.C. 20362 Attn: Mr. J. Murrin	1
Naval Sea Systems Command SEA-0332 Washington, D.C. 20362 Attn: Dr. A. Amster	1
Naval Surface Weapons Center Research and Technology Dept.-WR Silver Spring, MD 20910	1
Naval Weapons Center Research Department Code 60 China Lake, CA 93555	1
Naval Weapons Center Code 608 China Lake, CA 93555 Attn: Ronald L. Derr	3
Air Force Office of Scientific Research Directorate of Aerospace Sciences Bolling Air Force Base Washington, D.C. 20332	1
Air Force Office of Scientific Research Directorate of Chemical Sciences Bolling Air Force Base Washington, D.C. 20332	1
Air Force Office of Scientific Research Directorate of Physics Bolling Air Force Base Washington, D.C. 20332	1
U.S. Army Research Office Chemistry Division P.O. Box 12211 Research Triangle Park, N.C. 27709	1
U.S. Army Research Office Physics Division P.O. Box 12211 Research Triangle Park, N.C. 27709	1
Professor S.N.B. Murthy Technical Director, Project SQID Purdue University Lafayette, IN 47907	5

Collisional Relaxation of Transient Vibrational Energy Distributions in a Thermal Unimolecular System.[a] The Variable Encounter Method.

D. F. Kelley, L. Zalotai[b] and B. S. Rabinovitch

Department of Chemistry BG-10, University of Washington

Seattle, WA 98195

Abstract

A method has been developed, called the Variable Encounter Method, for the study of the relaxation of an initial vibrationally cold ensemble of molecules into a vibrationally hot distribution by a known and variable number of successive collisions with a hot wall. The theory of the experiment is presented. The system studied was the isomerization of 1,1,cyclopropane-d_2 with a fused quartz wall temperature of 800 K to 1175K, and average number of collisions from 2.3 to 22.3. Various modified gaussian and exponential models of energy transfer were found to give agreement with the data. The average down-step size was found to decline from $\lesssim$ 3500 cm^{-1} at the lowest temperature to $\sim$ 2500 cm^{-1} at the highest on the basis of a gaussian model. A mathematical analysis of the relation between mean first passage times and incubation times is given. Incubation times increase from $\sim$ 7 to $\sim$ 12 collisions with increasing temperature. Transient population distributions and the sequential reaction probabilities as a function of collision number are calculated.

I. INTRODUCTION

There have been no previous measurements of the dynamics of the collisional relaxation of vibrationally excited polyatomic molecules. If an ensemble of reactant molecules embedded in a hot bath gas starts out in a "cold" distribution, whether Boltzmann or not, it will relax by collisions with the bath gas molecules to a steady-state "hot" distribution. The study of reaction probabilities associated with the intermediate distributions can provide insights into the form of the energy transfer distribution function over the entire range of energies from 0 to E_o, the reaction threshold. One may thus determine the entire matrix of collision energy transfer probabilities $\underset{\sim}{P}$. The probability matrix also appears in expressions for the mean first passage time, $\bar{t}_{fp}$, of molecules with respect to an absorbing barrier, as given by Kim[1] and Widom.[2] In the trivial case of a constant temperature, steady-state, low pressure, unimolecular system, $\bar{t}_{fp} = 1/k_o$, where k_o is the low pressure rate constant.

Formal theoretical treatments of the transient in vibrational relaxation have been given for special assumed forms of $\underset{\sim}{P}$.[3,4] Usual treatments have considered the relaxation to be a continuous rather than discrete process. This is valid for the case of a fixed time interval between collisions only if the relaxation time is long compared to the time between collisions. This condition is not met for a reasonably strong collider. A general treatment then requires that the relaxation process be formulated in terms of difference rather than differential equations. The resultant difference equations, which are not tractable by any analytical technique, must be solved numerically.

A very simple method of study of the collision-by-collision relaxation of vibrational energy, i.e., of the relaxation transients, has been developed.[5,6] The collisions are with a wall which, in analogy with experimental results on homologous series of bath molecules of increasing size,[7] and on the basis of a

quasi-statistical model,[8,9] is anticipated to be at least as efficient as any gaseous bath molecule. In this technique a molecule experiences a large number of collisions with a cold wall of known, variable temperature and is brought into equilibrium with it before having a series of collisions (an encounter) with the hot walls of a reactor. By varying the geometry of the reactor, one can change the average number (and number distribution) of successive hot collisions, hence the name, Variable Encounter Method (VEM). Escape from the reactor, usually without reaction, leads to re-equilibration on the cold wall before re-entry into the hot reactor. The amount of reaction that occurs after a given number of encounters may be measured.

The reaction chosen for this study is the ring opening isomerization of 1,1-cyclopropane-d_2 to propene. This process has a critical threshold of about 64 kcal and a pre-exponential factor of $\sim 1.3 \times 10^{15}$ sec^{-1}. It has been studied in the homogeneous steady state case,[10] and a preliminary account of VEM work has been reported.[6] Light cyclopropane has also been used in VEM work to be reported.[5] This system was chosen not only because homogeneous studies of energy transfer at comparable temperatures with inert bath gases already exist,[10] but also because this reaction is well known to be notably free from complicating surface and wall seasoning effects.

II. EXPERIMENTAL

The apparatus consisted of a 5-liter fused quartz spherical flask which had several quartz cylindrical finger reactors of various dimensions blown onto the surface. Each finger, which could be heated separately, consisted of a cylindrical region of length ℓ, terminated by a hemisphere of radius r which varied from 2.1 to 2.5 cm for different reactors. The ratios of ℓ/r for the reactors used are given in Table I. The entrance area to a reactor was $\sim$ 1% of the total area of the flask. The reactor could be enclosed in a stainless steel heater block which was heated by clamshell Kanthal ceramic heaters. Fine silica sand was used as a thermal conduction medium in the approximately 2-3 mm gap between the quartz reactor and the steel block. Temperature measurements were made with several chromel-alumel thermocouples glued onto the outside of the reactor finger. Typical reactor temperatures were 750K to 1150K, while flask temperatures were 350K to 400K.

Some temperature gradients over the reactor surface, particularly near the attachment to the cold flask, were unavoidable. This problem was substantially reduced by having additional heaters embedded in the top of steel block. In this way, the reactor temperature could be maintained constant to $\pm$ 5° within a distance of $\sim$ 0.7 cm from the top of the reactor where the temperature commenced a more abrupt decline. The temperature profile over the longer reactors (where radiation losses were not so great) could be maintained constant within 2°-3°. Thus, an uncertain area of reduced temperature amounted to $\sim$ 10-15% for the smallest reactor and was negligible for the longer reactors. Calculations indicate that temperature gradients through the quartz wall ($\sim$ 2 mm thick) were completely negligible.

p. 3a

A pre-exposure of the oxidized quartz surface to the substrate, at a pressure of about 5×10^{-4} torr deposited a thin film of "polycyclopropane" on the surface and provided reproducible results for the measured rates of isomerization. The seasoning time required to achieve reproducible results was somewhat longer than in conventional static systems (i.e., hours and days, rather than minutes or hours). Prior to a run, the system was pumped down to $< 10^{-6}$ torr, the reactant was introduced at a pressure usually equal to $1\text{-}2 \times 10^{-4}$ torr, although experiments were made over the range $0.5\text{-}9.0 \times 10^{-4}$ torr. Run times varied from $\sim$ 10 minutes to several hours with the amount of reaction being 1-50%.

Analysis was by gas chromatography with a squalane SCOT column and a flame ionization detector.

III. CALCULATIONAL TECHNIQUE

1. Calculation of "number of collisions" distribution per encounter

There is a distribution $\underset{\sim}{n}$ of the number of collisions made by a molecule with the wall after entering the reactor (an encounter). The distribution $\underset{\sim}{n}$ was changed by changing the ℓ/r ratio; in this work, ℓ/r varied from 0.17 to 10. This distribution was obtained by a stochastic calculation of the acutal trajectories of single molecules. In the calculation of $\underset{\sim}{n}$, it was assumed that the surface is rough on the molecular level, so that a cosine law distribution of angular reflection is valid after each collision regardless of incident trajectory. (If this assumption were replaced by one of specular reflection, it would result in only a modest change in $\underset{\sim}{n}$. The details of this calculation are now given.

Molecules which cross the boundary plane separating the reactor finger from the bulb do so with an angular distribution function

$$P(\theta) = 2 \sin\theta \cos\theta , \qquad (1)$$

where $P(\theta)$ is defined as the normalized probability of a molecule trajectory making an angle θ with respect to the normal to the plane. This cosine law distribution is the general result for effusive molecules. Actually, at typical operating pressure, the mean free path is comparable to the dimensions of the spherical flask. However, the same result is obtained by integrating over the surface of the flask (see App. A).

The z axis is chosen along the axis of the cylinder; $z = 0$ defines the plane separating the hemispherical and cylindrical parts of the reactor finger, with z positive in the hemisphere. The x_o and y_o coordinates on the $z_o = -\ell/r$ plane (separating the cylinder from the large flask) are chosen randomly for

any one molecule, such that $x_o^2 + y_o^2 \leq 1$, in units of r. The initial trajectory of the molecule is defined by x_o and y_o, by θ, chosen randomly to conform to eq. 1, and by an azimuthal angle ϕ, chosen randomly between 0 and 2π. This trajectory may be written as

$$(x(t),y(t),z(t)) = (x_o,y_o,z_o) + t(x',y',z') \qquad (2)$$

where t is a (continuous) parameter, and $x' = \sin\theta\cos\phi$, $y' = \sin\theta\sin\phi$, $z' = \cos\theta$. This trajectory may intersect the reactor in either the cylinder or the hemisphere; the two cases are handled separately. In either case, one calculates the first impact coordinates (x_1,y_1,z_1). To obtain the new set of coordinates (x",y",z"), which define the next trajectory analogous to eq. (2), one first defines a transformation such that,

$$\begin{pmatrix} 1 \\ 0 \\ 0 \end{pmatrix} = \underset{\sim}{T} \begin{pmatrix} x_1 \\ y_1 \\ z_1 \end{pmatrix} ;$$

the new coordinates are then given by,

$$\begin{pmatrix} x'' \\ y'' \\ z'' \end{pmatrix} = \underset{\sim}{T}^{-1} \begin{pmatrix} 1-\cos\theta \\ \sin\theta\sin\phi \\ \sin\theta\cos\phi \end{pmatrix},$$

where θ and ϕ are chosen in the same manner as for the initial trajectory. For the case of the impact on the hemisphere, the matrix representation of $\underset{\sim}{T}$ is given by a product of rotations,

$$\underset{\sim}{T} = \begin{pmatrix} \cos\psi & 0 & \sin\psi \\ 0 & 1 & 0 \\ -\sin\psi & 0 & \cos\psi \end{pmatrix} \begin{pmatrix} \cos\alpha & \sin\alpha & 0 \\ -\sin\alpha & \cos\alpha & 0 \\ 0 & 0 & 1 \end{pmatrix} ;$$

$\psi = \sin^{-1}(z_1)$; $\alpha = \tan^{-1}(y_1/x_1)$. For impact on the cylinder, $\underset{\sim}{T}$ is a product of a rotation about the z axis and a translation. The next impact point is found, with consideration, also, of the possibility of escape from the finger.

This process is repeated until the molecule escapes. In this way, the distribution $\underset{\sim}{n}$ is determined by calculating many trajectories (1000-5000, practise). An average inter-collision free flight distance is also obtained.

From $\underset{\sim}{n}$, it is useful to define a correlation table for each reactor,

$$C_j = \sum_{i=j+1}^{\infty} n_i \Big/ \sum_{i=j}^{\infty} n_i$$

C_j is defined as the probability that a molecule will have at least j+1 collisions given that it has j, i.e., the probability that a remaining molecule will not escape after the jth collision (Table I). The average number of collisions per encounter, m, is recovered from the correlation table by the expression:

$$m = \sum_{j=1}^{\infty} j \left(\prod_{i=1}^{j-1} C_i \right) \left(1 - C_j \right)$$

After a few collisions, the molecule "forgets" the initial conditions and the correlation table asymptotically approaches a constant. The number of collisions required to reach this limit, within statistical fluctuations introduced by the stochastic nature of the calculation, varies from 0, for the shortest reactor, to about 15, for the longest.

2. Simulation of the "collision" process. Models for energy transfer

A normalized Boltzmann population vector $\underset{\sim}{N}$, characteristic of the flask temperature, is constructed to represent the molecules that enter the reactor. To simulate a collision, this vector is operated on by the probability matrix. After each wall collision, the population of each molecular energy level changes until an equilibrium distribution (or steady state if reaction is considered) is realized. The population of the ith level after collision, N_i', is given by

$$N_i' = \sum_{j=0}^{\infty} p_{ij} N_j$$

where N_j is the population of the jth level before the collision, and p_{ij} is the probability per collision of a transition from the jth level to the ith level. This equation may be written in matrix form $\underset{\sim}{N}' = \underset{\sim}{P}\,\underset{\sim}{N}$. Since no change takes place after an equilibrium distribution of molecules is established,

$$(\underset{\sim}{P} - \underset{\sim}{1})\,\underset{\sim}{N}_{eq} = \underset{\sim}{0} \tag{3}$$

The following constraints thus apply to the $\underset{\sim}{P}$ matrix,

$$p_{ij}/p_{ji} = (g_i/g_j)\exp[-(E_i-E_j)/RT]$$

$$\sum_{i=o}^{\infty} p_{ij} = 1$$

where g_i is the degeneracy of the ith level.

Since there are, of course, far too many levels to permit their enumeration, the levels are grouped together, usually in "grains" of 100 cm^{-1}. If we now specify the form (model) of the down transitions, this will completely specify the matrix $\underset{\sim}{P}$. Further details of the construction of this matrix are given in ref. (11). In the calculations two different models for the probability of a given down transition, ΔE, were used:

exponential: $P_{\Delta E} = A\exp(-\Delta E/\langle\Delta E\rangle)$; $0 \le \Delta E \le 9000\ cm^{-1}$;

$= 0$; $\Delta E > 9000\ cm^{-1}$;

gaussian: $P_{\Delta E} = A'\exp[-(\Delta E-\Delta E_{mp})^2/2\sigma^2]$; $0 \le \Delta E \le 9000\ cm^{-1}$;

$= 0$; $\Delta E > 9000$;

where the limitation $\Delta E < 9000\ cm^{-1}$ is a practical computational feature to limit the total size of the matrix to tractable dimensions; A and A' are normalization constants which also depend on the up transitions; $\langle\Delta E\rangle$, ΔE_{mp} (mp signifies most probable), and σ are parameters of the model. We note that on the exponential model, if $\langle\Delta E\rangle \ll 9000$ then the effective size of the average down transition $\langle\Delta E'\rangle$

is simply $\langle\Delta E\rangle$. For the gaussian model, if $\sigma << \Delta E_{mp}$ then this effectively becomes a stepladder model and $\langle\Delta E'\rangle = \Delta E_{mp}$; if $\sigma \geq \Delta E_{mp}$ then there is a fairly large probability for elastic or near-elastic transitions, and this form begins to resemble a poisson model.

In the case of the exponential model, $\langle\Delta E\rangle$ (or ΔE_{mp} in the case of the gaussian) was also allowed to vary with initial energy in some calculations. This dependence was given by $\langle\Delta E\rangle = \alpha + \beta E^{x}$, with the same expression for ΔE_{mp}, where α, β, and x are adjustable parameters. Most thoroughly studied were the cases where $\beta = 0$, α adjustable (a "flat" model), and $\alpha = 500$, β adjustable, $x = 1$ (a "linear" model). (α is not chosen to be zero in the linear model to avoid a singularity in the construction of the matrix). In all cases, down transitions larger than the initial energy were treated as elastic. The probability matrices so constructed conform to eqs. 3 and 4.

In the limit of a strong collider, one expects a Boltzmann distribution to result from every energy level of the initial distribution,in one collision. To transform the molecules initially at high energy into a Boltzmann distribution requires a larger down step than is required for molecules initially at lower energy. Thus,linear models have some pretension to greater physical content than do flat models.

3. Simulation of the entire encounter process

Between successive wall collisions, say the jth and j+1th, the population vector must be attenuated for loss due to reaction and escape. The ith element in the vector is modified by

$$N_i' = C_j \, e^{-k_i \tau} N_i$$

where C_j is the jth element in the correlation table; k_i is the microscopic RRKM rate constant at energy, E_i ; and τ is the average intercollision time obtained

from the average intercollision distance, assuming translational velocity characteristic of surface temperature. The vibrational parameters used in the RRKM calculation of k_i as a function of energy are given in App. B. This collision-attenuation process is repeated until the vector $N_i \cong 0$ for all i, or until some extrapolation procedure may be used (see App. C). The amount of reaction after each collision is then

$$P_j' = \sum_i N_i[C_j(1-e^{-k_i\tau}) + (1 - C_j)(1-e^{-k_i\tau'})]$$

where τ' is the average flight time before a gas-gas or cold wall collision after a molecule leaves the reactor finger, both treated on a fixed gap basis. In this system, the effective pressure is sufficiently low so as to make the calculation of P_j' insensitive to the fixed gap approximation, or to any reasonable error in the calculation of the k_i. The average probability of reaction per collision is given by $\bar{P}_c(m) = \sum_j P_j'/m$.

V. Results and Discussion

1. $P_c(m)$ as a function of m and temperature.

Figure 1 presents the experimental average probability of reaction per collision $\bar{P}_c(m)$ versus temperature for the five reactors. Least-squares quadratic fits are shown; the corresponding Arrhenius plots are given in Fig 2. Values of the observed activation energies are summarized in Table II. If the wall were a strong collider, there would be no transient, and all $\bar{P}_c(m)$ curves would coincide. (Related behavior in strong collider low-pressure thermal unimolecular theory is that the rate of reaction of substrate embedded in a bath gas at temperature T is independent of the initial energy distribution of substrate molecules below the critical threshold E_o.) Figure 3 shows the least squares fit curves and comparison with several calculated curves. In all cases, $\langle\Delta E'\rangle$ was adjusted to fit the m = 2.3 curve, at temperatures where such data was available.

Several features of the calculated curves reveal themselves:

a) The calculated value of $\bar{P}_c(m)$ is a more sensitive function of $\langle\Delta E'\rangle$ for the smaller reactors. This is the reason why $\langle\Delta E'\rangle$ was in all cases adjusted to fit the data from the m = 2.3 reactor where available. (It should be kept in mind, however, that this reactor is probably the one most susceptible to experimental error, i.e., temperature measurement and gradients over the surface.)

b) For small m, i.e., the case for the first few collisions when relatively more of the molecules are at low energy, the exponential model is more efficient. This is due to its relatively greater probability of very large up jumps; this, in turn, permits a larger contribution to reaction after only a few collisions than do the gaussian distributions so that a relatively smaller value of $\langle\Delta E\rangle$ is required in order to fit the m = 2.3 data. For large m, by contrast, more molecules have moved up to higher energies near E_o (Figs. 4-6) and gaussian

models give larger values of $\bar{P}_c(m)$ than do exponential models; the reason for this is the high probability of near-elastic collisions associated with the exponential model. Similar effects may also be seen (Fig. 3) upon comparison of the two gaussian models characterized by different σ, where the one with larger σ has properties more closely related to an exponential distribution.

Linear models give higher values of $\bar{P}_c(m)$ than do the corresponding flat models for large m reactors. The reason for this is that the linear model has a lower $\langle\Delta E'\rangle$ at low energies (Figs. 4-6) and a smaller probability of effecting transitions from these to energies above E_o (so that a larger value of $\langle\Delta E'\rangle$ is required, to fit the data for the m = 2.3 reactor). For large m, the higher $\langle\Delta E'\rangle$ associated with the linear model at higher energies enhances the reaction probability compared to the flat model. The two effects mentioned above produce the result that the linear exponential and flat gaussian (σ = 0.7 ΔE_{mp}) curves are virtually coincidental.

As can be seen from Figure 3, three different models all give adequate (within experimental error) fit to the data. The best fit seems to be obtained with the flat gaussian (σ = 0.7 ΔE_{mp}) model and the linear exponential model. The flat gaussian models with σ = 0.35 ΔE_{mp} give poorer fit and are somewhat above the experimental curves. The linear gaussian models (not shown) lie slightly above the corresponding flat models, especially at higher temperature.

c) Regardless of the model, two findings emerge: i) $\langle\Delta E'\rangle$ drops significantly with increasing temperature; and ii) $\langle\Delta E'\rangle$ for wall collisions is greater than $\langle\Delta E\rangle$ for gas-gas collisions (see Table III). This drop of $\langle\Delta E\rangle$ with temperature is the reason why the $\bar{P}_c(m)$ curves separate more at higher temperatures. At lower temperatures, one loses resolution between the models as they all approach closer to the strong collider behavior.

2. Sequential reaction probabilities and population distributions

The form of $\bar{P}_c(m)$ may be written as

$$\bar{P}_c(m) = \frac{1}{m} \sum_{j=1}^{\infty} P(j) \prod_{i=0}^{j-1} C_i \, (1-P(i))$$

where C_i is the ith entry in the correlation table; thus the continued product represents the fraction of reactant molecules left after j-1 collisions; P(j) is the sequential reaction probability, i.e., the probability of reaction after the jth wall collision made by a molecule. Plots of P(j) for various models are given in Fig. 7. The smaller m reactors weight the small j values of the P(j) more than do the larger m reactors. Thus, additional explanations to the effects discussed in the previous section may be seen in terms of these plots. The reason that the $m = 2.3$ reactor is much more sensitive to changes in $\langle \Delta E' \rangle$ than the larger in reactors is due to the fact that P(j) is much more sensitive to changes in $\langle \Delta E' \rangle$ at small j than at large j. That is, the rate of relaxation is much more sensitive to changes in $\langle \Delta E' \rangle$ than is the value to which it relaxes. This has been found to be true for all models.

The relative and absolute population distributions, which formed some basis for the discussion in the previous section, are shown in Figs. 4-6. Examination of these figures shows that the population distribution is very significantly altered after one collision. As a consequence, for these fairly strong collisions, the reaction rate should be quasi-independent of input distribution (flask temperature). This was found to be the case experimentally when the flask temperature was raised by 100° without effect.

It is also clear from these distributions that the average energy approaches its steady state value rather rapidly. This is due, in part, to the fact that there is a very large average upstep at low energies. The large upstep is a result of detailed balance at low energy levels where the densities of molecular

states change very rapidly with energy. A related conclusion is that the "temperature", as determined by the bulk of the population distribution, relaxes much more quickly than does the population around E_o, i.e., than does the reaction rate. In the case of the gaussian model ($\sigma = 0.7\ \Delta E_{mp}$) at high temperature, this upstep is so large that the value of E_{mp} after one collision overshoots the steady state value a little (Fig. 4). Despite the fact that this gaussian model works well, we question how physically reasonable this result can be. Indeed, as σ was made smaller, other non-physical calculational results were obtained at lower energies with the gaussian models. For $\sigma = 0.17\ \Delta E_{mp}$, $P(j)$ ceased to be a monotonic function of j. For the present system, in which the energy range of interest varies from zero upward, a simple step ladder model is quite unsatisfactory. This is in contrast to chemical activation systems, where only energies around, or above, E_o play an important role. A variety of additional population distributions for all models discussed have been calculated and may be found in ref. 6b.

The relative decline in the Arrhenius activation energy with decrease in m (Table II) illustrates the relative effect of increasing population depletion, at higher energies, with rise of temperature in the transient regime.

3. Mean first passage time and the "incubation" time

The first mean passage time, $\bar{t}_{fp}$, as developed by Kim[1] and Widom[2] gives the average amount of time required for a molecule to attain an energy equal to or greater than E_o as

$$\bar{t}_{fp} = \int_0^\infty t\ p(t)\ dt\ ; \qquad (5)$$

where $p(t)$ is the normalized probability that a molecule will cross E_o, for the first time, at time t. $\bar{t}_{fp}$ is a molecular property and is independent of m. Clearly, $\bar{t}_{fp}$ is a well-defined quantity at all pressures but is most simply related to the actual rate of reaction in the low pressure limit of a unimolecular system. If the system is at low pressure, $p(t)$ is the probability of reaction at time t, which is the case we now consider and to which our system approximates.

Equation 5 may be written as a sum

$$\bar{t}_{fp} = \sum_{j=1}^{\infty} jP(j) \prod_{i=o}^{j-1} (1-P(i))$$

where time is measured in units of collision intervals, and the continued product is the fraction of unreacted molecules after j-1 collisions, and Δt is unity

We define an "incubation" time in terms of mean first passage times,

$$\tau_{inc} = \bar{t}_{fp} - \bar{t}_{fp}^{ss}$$

where $\bar{t}_{mf}^{ss}$ is the steady state mean first passage time, and $\bar{t}_{fp}$ is the mean first passage time for the case of transients. It is shown in Appendix D that

$$\tau_{inc} = \lim_{j \to \infty} (j - \sum_{i=o}^{j-1} P(i)/P) + O(j^{\dagger 2}P) \qquad (6)$$

where P is $P(\infty)$, and $j^{\dagger}$ is a characteristic relaxation time for the system, and $P(j^{\dagger}) \gtrsim 0.6P$. In most cases, the second term of eq. 6 is small; in the present case, it is $\sim$ 10^{-4} - 10^{-7} of the first. So for this case, we may write

$$\tau'_{inc} = \lim_{j \to \infty} (j - \sum_{i=o}^{j-1} (P(i)/P)) \qquad (7)$$

Dove and Troe [12] define an incubation time τ_{inc}^{DT} in shock systems by the equation

$$N(t)/N(o) = \exp[-P(\infty)(t-\tau_{inc}^{DT})] \qquad (8)$$

where N(t) is the concentration of reactant at time t, and where eq. (8) is to be evaluated at sufficiently large t so that all transients have disappeared. It is shown in Appendix D that τ_{inc}^{DT} is simply the special case τ'_{inc} (eq. 7). Calculated values for τ'_{inc} are given in Table IV.

Conclusions

For the temperatures studied in this system, relaxation approaches the steady state in a small number of collisons $\sim$ 10-20 (Fig. 4) with corresponding incubation times of 7-13 collisions (Table IV). This accounts for the finding of steady state behavior in low pressure pyrolysis studies[14] where $m \gtrsim 80\text{-}100$.

Adequate agreement with the data is obtained with flat exponential, linear exponential, and flat gaussian ($\sigma = 0.7\Delta E_{mp}$) models. The best agreement is with linear exponential and flat gaussian models whose calculated $P_c(m)$ curves are essentially indistinguishable. The flat gaussian ($\sigma = 0.35\Delta E_{mp}$) linear gaussian and stepladder models do not give adequate agreement.

Wall collisions are more efficient than gas phase collisions; a quartz surface seasoned with a film of "polycyclopropane" is characterized by down step sizes of $\sim$ 3800 and 2950 cm^{-1} (flat gaussian model, Table III) at 800K and 975K, respectively. These compare with lesser values of $\sim$ 3300 and 1900 cm^{-1} deduced previously on a stepladder model for neat cyclopropane-d_2 gas phase collisions at the same temperatures (note these values would decline somewhat on a gaussian model basis).

The data of this study also support the previous finding[10] that, in the temperature range investigated, energy transfer collisional efficiency declines at higher temperatures in polyatomic molecule systems.

Table I. Correlation Tables, C_n, for Various Reactors

ℓ/r	0.17	0.46	1.45	4.0	10.0
n\m	2.3	2.9	5.0	10.5	22.3
1	0.566	0.659	0.750	0.755	0.759
2	.566	.660	.788	.829	.833
3	⋮	.661	.800	.882	.889
4	⋮	.661	.809	.901	.908
5		⋮	.815	.915	.922
6		⋮	.819	.923	.933
7			.822	.928	.942
8			.824	.930	.950
9			.824	.931	.958
10			⋮	.931	.963
11			⋮	⋮	.968
12				⋮	.972
13					.975
14					.978
15					.979
16					.980
17					⋮

Table II. Apparent Arrhenius Activation Energies

	m				
	2.3	2.9	5.0	10.5	22.3
E_a(kcal mole^{-1})	not defined	35.5	42.5	48	50

Table III. ΔE Values for Various Models (cm^{-1})

		T (K)					
Model		825[1]	900	950	1025	1100	1150
flat exponential	$\langle\Delta E\rangle$	~10000	4300	4000	3000	2550	2300
	$\langle\Delta E'\rangle$	~ 6500	3035	2940	2685	2280	2115
linear exponential[2]	$\langle\Delta E\rangle$	~22000	6900	5890	4765	3870	3420
	$\langle\Delta E'\rangle$	~ 7800	3500	3400	3160	2900	2720
	β	~ 1.0	0.285	0.24	0.19	0.15	0.13
flat gaussian $\sigma = 0.35\ \Delta E_{mp}$	ΔE_{mp}, $\langle\Delta E'\rangle$	3500	3200	3100	2930	2700	2530
flat gaussian $\sigma = 0.7\ \Delta E_{mp}$	ΔE_{mp}	3200	2800	2700	2540	2330	2175
	$\langle\Delta E'\rangle$	3500	3100	2990	2810	2580	2410

[1] ΔE's at this temperature were selected to fit m = 10.5 curve since data for m = 2.3 was not available. Also, for exponential calculations, the maximum ΔE (matrix truncation) is chosen to be 18,000 cm^{-1} and the grain size to be 200 cm^{-1}; otherwise the customary 9,000 cm^{-1} and 100 cm^{-1} were used.

[2] ΔE values given at the level of energy, E_o .

Table IV. Incubation times, τ'_{inc} (number of collisions)

Model	900K	1150K
flat gaussian ($\sigma=0.7\Delta E_{mp}$)	6.5	10.7
flat exponential	7.4	12.3
linear exponential	8.0	13.3

Appendix A. Derivation of Angular Distribution Function for Entry in the Reactor

Consider a spherical polar coordinate system (r,θ,ϕ) centered in the large flask. The surface separating the reactor finger from the flask (which for this purpose is taken to be a differentially small plane of area A) is at the point $\theta = 0$; the radius is normalized to unity. We examine the low pressure case where gas-gas collisions may be ignored and derive the angular distribution of molecules hitting A assuming a cosine law distribution of molecules coming off the surface of the flask.

Now consider molecules that leave the sphere from the angular ring θ to $\theta + d\theta$ and hit A. This ring has area $2\pi\sin\theta\, d\theta$. The angle between A and the origin of the coordinate system as seen from any point on the ring at θ is given by

$$\psi = (\pi-\theta)/2 \qquad \text{(A1)}$$

The fraction of molecules that leave this ring and hit A is

$$df = 2\cos\psi\, d\Omega/2\pi \qquad \text{(A2)}$$

where $d\Omega$ is the solid angle subtended by A. (Note that if $d\Omega$ is set equal to the "volume element" $2\pi\sin\psi\, d\psi$ then $\int_0^{\pi/2} df = 1$ so eq. A2 is normalized.) For the geometry under consideration, $d\Omega = A\cos\psi/r^2$, where r is the distance between the ring and A, and $r = \sin\theta/\sin\psi$, so that

$$df = \frac{A}{\pi}\cos^2\psi\,\frac{\sin^2\psi}{\sin^2\theta}$$

This fraction, multiplied by the area of the ring and divided by A, gives the fraction of molecules incident between ψ and $\psi + d\psi$,

$$P(\psi)d\psi = \frac{1}{\pi}\frac{\cos^2\psi\,\sin^2\psi}{\sin^2\theta}\left(2\pi\sin\theta\,\frac{d\theta}{d\psi}\,d\psi\right)$$

Using eq. A1, this simplified to,

$$P(\psi)d\psi = 2 \cos\psi \sin\psi \, d\psi$$

which is the cosine distribution with the appropriate volume element, as desired. Although this distribution was derived assuming A to be infinitesmal, it holds approximately for finite A, provided A is sufficiently small so that the element of spherical surface of the flask may be approximated as a plane on A.

Appendix B. Vibrational Frequencies for RRKM Calculations (cm^{-1}).

1,1-Cyclopropane-d_2 molecule:

3100, 3080, 3040, 3020, 2330, 2210, 1480, 1350, 1180, 1130, 1110 (2).
1070, 1030, 1020, 980, 850, 810, 770, 620, 590.

Activated complex:

3020 (4), 2200 (2), 1440, 1400, 1050, 1200, 980 (2), 930, 920, 880, 750,
620, 600, 560, 460.

Appendix C. Extrapolation Method

The total probability of reaction per encounter may be written as

$$P_{enc} = m\bar{P}_c(m) = \sum_{j=1}^{\infty} P(i) \left(\prod_{i=o}^{j-1} C_i (1-P(i)) \right) \qquad (C1)$$

where C_i is the ith element in the correlation table ($C_o = 1$);
$\prod_{i=o}^{j-1} C_i(1-P(i))$ is the fraction of molecules that have at least j collisions.
$P(i)$ is the sequential reaction probability.

$P(j)$ is a monotonically increasing function of j that asymptotically approaches a limiting value, $P(\infty)$. For large enough j, called j^*, the approach to $P(\infty)$ can be described by the difference equation,

$$P(k+j^*) = P(k+j^*-1) \left[1 + R_{j^*} \left(\frac{R_{j^*}}{R_{j^*-1}} \right)^k \right] , \qquad (C2)$$

where R_{j^*} and R_{j^*-1} are defined by the following equations

$$P(j^*-1) = P(j^*-2)\ (1 + R_{j^*-1}) \ ,$$

and, similarly,

$$P(j^*) = P(j^*-1)(1 + R_{j^*}) \ .$$

One does the iterative simulation up to j^*, calculates R_{j^*-1} and R_{j^*}, and then uses the extrapolated values of P(j) in C1. It is found that eq. C2 works quite well if one chooses j^* such that $R_{j^*} \leq 0.01$. This corresponds in the present study to a j^* of about 15 to 30. We note also that eq. C2. implies a simple exponential relaxation to $P(\infty)$ when $R_{k+j^*} << 1$.

Appendix D. Incubation Time From First Mean Passage Time.

The incubation time is defined as the difference of mean first passage times with and without the transient,

$$\tau_{inc} = \bar{t}_{fp} - \bar{t}_{fp}^{ss} \quad .$$

For time measured in units of collisions,

$$\tau_{inc} = \sum_{j=1}^{\infty} jP(j) \prod_{i=o}^{j-1} (1-P(i)) - \sum_{j=1}^{\infty} jP(1-P)^j \quad , \tag{D1}$$

where P is $P(\infty)$.

These sums may be performed directly; however, they converge very slowly so that this becomes computationally undesirable. The following technique may be used to approximate the sum to any desired level of accuracy. We define j' such that P(j') has virtually converged on P and, recognizing that the second term contains a binomial expansion of $1/P^2$, we rewrite eq. D1 as

$$\tau_{inc} = \sum_{j=1}^{j'} jP(j) \prod_{i=o}^{j-1} (1-P(i)) + P \sum_{j=j'+1}^{\infty} j(1-P)^{j-j'} \prod_{i=o}^{j'-1} (1-P(i)) - (1-P)/P. \tag{D2}$$

We note that $t_{fp}^{ss} = (1-P)/P \cong 1/P$ (where t_{fp}^{ss} is not exactly 1/P because an integral was replaced by a discrete sum). Adding and subtracting to the second term of eq. D2,

$$\tau_{inc} = \sum_{j=1}^{j'} jP(j) \prod_{i=o}^{j-1} (1-P(i)) + P \prod_{i=o}^{j'-1} (1-P(i))(1-P)^{-j'} \left[(1-P) \sum_{j=1}^{\infty} j(1-P)^{j-1} - \sum_{j=1}^{j'} j(1-P)^j \right] - (1-P)/P \quad ,$$

or

$$\tau_{inc} = \sum_{j=1}^{j'} j \left[P(j) \prod_{i=o}^{j-1} (1-P(i)) - P\left(\prod_{i=o}^{j'-1} (1-P(i)) \right) (1-P)^{j-j'} \right] + \frac{1}{P} \left[(1-P)^{1-j'} \prod_{i=o}^{j'-1} (1-P(i)) \right] - (1-P)/P \, . \tag{D3}$$

Of course, eq. D3 must be exactly equal to eq. D1 if one lets $j' \to \infty$ (so $P(j') = P$ exactly), but is calculationally tractable because the sum converges for relatively small values of j';(in the first term of eq. D3, terms in the sum approach zero, and in the second term, factors in the product approach unity, as $j' \to \infty$; evaluation of eq. D1 would require 10^5 to 10^8 terms whereas eq. D3 requires only 30 to 60). Equation D3 may be simplified further by expanding in a power series in P (all P(j) are considered to be of order P). After some manipulation with use of the binomial expansion of $(1-P)^{1-j'}$ and the relation,

$$\prod_{i=o}^{j'-1} (1-P(i)) = 1 - \sum_{i=o}^{j'-1} P(i) + \sum_{i=o}^{j'-1} P(i) \sum_{i'=o}^{i-1} P(i') + \cdots ,$$

eq. D3 becomes

$$\tau_{inc} = \lim_{j' \to \infty} \left[j' - \sum_{i=o}^{j'-1} P(i)/P \right] + R + O(P^2) , \qquad (D4)$$

where

$$R = \lim_{j' \to \infty} R_{j'} = \lim_{j' \to \infty} \sum_{j=1}^{j'} j(P(j)-P) + j'(j'-1)P/2 + (1-j') \sum_{i=o}^{j'-1} P(i) + \sum_{i=o}^{j'-1} P(i) \sum_{i'=o}^{i-1} P(i')/P .$$

Clearly, R is of order P. If P were large, such that the $O(P^2)$ term should be evaluated, then eq. D3 should be used. If P is sufficiently small, eq. D4 becomes simply

$$\tau'_{inc} = \lim_{j' \to \infty} \left(j' - \sum_{i=o}^{j'-1} P(i)/P \right) \qquad (D5)$$

In the present study, P is 10^{-5} to 10^{-8}, so, as will most often be the case, eq. D5 is entirely adequate.

To examine the intermediate case, we ignore all terms $O(P^2)$ and derive a more explicit estimate of the magnitude of R. We write $R = \sum_{j=1}^{\infty} (R_j - R_{j-1})$; in terms of this sum R is,

$$R = \lim_{j' \to \infty} \sum_{j=1}^{j'} [j(P(j)-P(j-1)) + P(j-1) - P - (1-P(j-1)/P) \sum_{i=0}^{j-2} P(i)] \qquad (D6)$$

R may be readily calculated for the important special case of exponential relaxation of the transient, i.e., $P(j) = P(1-e^{-j/j^{\dagger}})$. If the relaxation is not too fast, then we may replace the sums in eq. D6 by integrals. (Replacing the sum by an integral in eq. D5 in this case gives $j^{\dagger} \simeq \tau'_{inc}$.) The first two terms of eq. D6 cancel and we are left with $R \simeq \int_0^{\infty} P(j')/P-1) \int_0^{j'} P(j)djdj'$, or $R \simeq -\frac{1}{2} j^{\dagger 2} P$. In general, we find R is $O(j^{\dagger 2} 0)$, where $j^{\dagger}$ is the characteristic relaxation time of the transient. The exact relationship between $j^{\dagger}, \tau_{inc}$ and the j' necessary for convergence of eq. D3 varies with the nature of the relaxation process.

For the definition of τ_{inc}^{DT} given by eq. 8, it follows that (with time measured in collisions, see (Fig. 8),

$$\tau_{inc}^{DT} = \lim_{j' \to \infty} j' + \frac{1}{P} \ln(N(j')/N(0) \quad .$$

But

$$- \ln N(j')/N(0) = \sum_{j=0}^{j'-1} P(j) \; ;$$

therefore,

$$\tau_{inc}^{DT} = \lim_{j' \to \infty} \left[j' - \sum_{j=0}^{j'-1} P(j)/P \right] = \tau'_{inc}$$

References

a) This work was supported by the Office of Naval Research and in part by the National Science Foundation.

b) UNIDO Fellow. University of Szeged, Szeged, Hungary.

1. S. K. Kim, J. Chem. Phys. 28 (1958) 1057
2. B. Widom, J. Chem. Phys. 31 (1959) 1387; 34 (1961) 2050
3. R. J. Rubin and K. E. Shuler, J. Chem. Phys. 25 (1956) 59, 68
4. E. W. Montroll and K. E. Shuler, Adv. Chem. Phys. 1 (1958) 361
5. B. D. Barton, Ph.D. Thesis, University of Washington, in preparation.
6. a) D. F. Kelley, B. D. Barton, L. Zalotai and B. S. Rabinovitch, J. Chem. Phys. 71 (1979); b) D. F. Kelley, Ph.D. thesis, to be presented.
7. S. C. Chan, B. S. Rabinovitch, J. T. Bryant, L. D. Spicer, T. Fujimoto, Y. N. Lin and S. P. Pavlou, J.Phys. Chem. 74 (1970) 3160; D. C. Tardy and B. S. Rabinovitch, Chem. Revs. 77 (1977) 369
8. Y. N. Lin and B. S. Rabinovitch, J. Phys. Chem. 74 (1970) 3151
9. W. Eastes and J. P. Toennies, J. Chem. Phys. 70 (1979) 1644
10. I. E. Klein and B. S. Rabinovitch, Chem. Phys. 35 (1978) 439
11. D. C. Tardy and B. S. Rabinovitch, J. Chem. Phys. 45 (1966) 3720
12. J. E. Dove and J. Troe, Chem. Phys. 35 (1978) 1
13. J. E. Dove, W. S. Nip and H. Teitelbaum, Intern. Sympos. Combust. 15 (1974) 903
14. G. N. Spokes and S. W. Benson, J. Am. Chem. Soc., 89 (1967) 2527; K. D. King, D. M. Golden, G. N. Spokes and S. W. Benson, Int. J. Chem. Kin. 3 (1971) 411

Figure Captions

Fig. 1 Plots of experimental values of $\bar{P}_c(m)$ vs T (K) for each of the five reactors. Solid curves are quadratic least square fits to each set of data. The m-number is attached to each set.

Fig. 2 Observed rate constants calculated from least square fit curves of Fig. 1 plotted vs reciprocal of absolute temperature. The m = 2.3 curve has too much curvature for the apparent activation energy to be well defined.

Fig. 3 Comparison of the experimental $\bar{P}_c(m)$ vs T least square fit curve (solid) for each reactor (Fig. 1) with curves calculated on the basis of various models: — · — , flat gaussian ($\sigma = 0.35\ \Delta E_{mp}$); —— – —— , linear exponential and flat gaussian ($\sigma = 0.7\ \Delta E_{mp}$) – – – , flat exponential. The linear exponential and flat gaussian ($\sigma = 0.7\ \Delta E_{mp}$) curves are essentially indistinguishable. The m = 10.5 curves are not shown to avoid cluttering of the graph; however, the relative positions of these curves are very similar to those for the m = 22.3 case. For each model, the ΔE value was chosen at a particular temperature so as to fit the m = 2.3 curve; the values are given in Table III.

Fig. 4 Histograms of the calculated sequential reaction probability P(n) vs n, the number of consecutive collisions. Calculations performed at a) 900K and b) 1150K with: ... , gaussian ($\sigma = 0.7\ \Delta E_{mp}$); ——— , linear exponential; and — — — , flat exponential models, with ΔE values indicated in Table III.

Fig. 5 a) Absolute population distributions N(E) vs E at 900K, portrayed after various numbers of collisions (attached to each curve) and calculated with linear exponential or (indistinguishable) flat gaussian ($\sigma = 0.7\ \Delta E_{mp}$) models. The curves on the right represent magnification of ordinate scale by a factor of 100. The n = 17 distribution closely approximates the steady state distribution.
b) Absolute population distributions N(E) vs E at 1150K calculated with the flat gaussian ($\sigma = 0.7\ \Delta E_{mp}$) model and portrayed after various numbers of collisions. The n = 21 distribution curve is essentially steady state. See caption (a).

Fig. 6 Absolute population distribution at 1150K calculated with the linear exponential model after various numbers of collisions. The n = 25 distribution approximates the steady state. See caption Fig. 5a.

Fig. 7 Relative population distributions $N(E)/N(E)_{eq}$ vs $E(cm^{-1})$ calculated with the linear exponential model at a) 900K and b) 1150K, portrayed after various numbers of collisions (attached to each curve). In both cases, the distribution of the last collision shown approximates the steady state distribution.

Fig. 8 Graphical representation of eq. 8. Solid curve is asymptotic to dashed line whose slope is steady state reaction rate P .

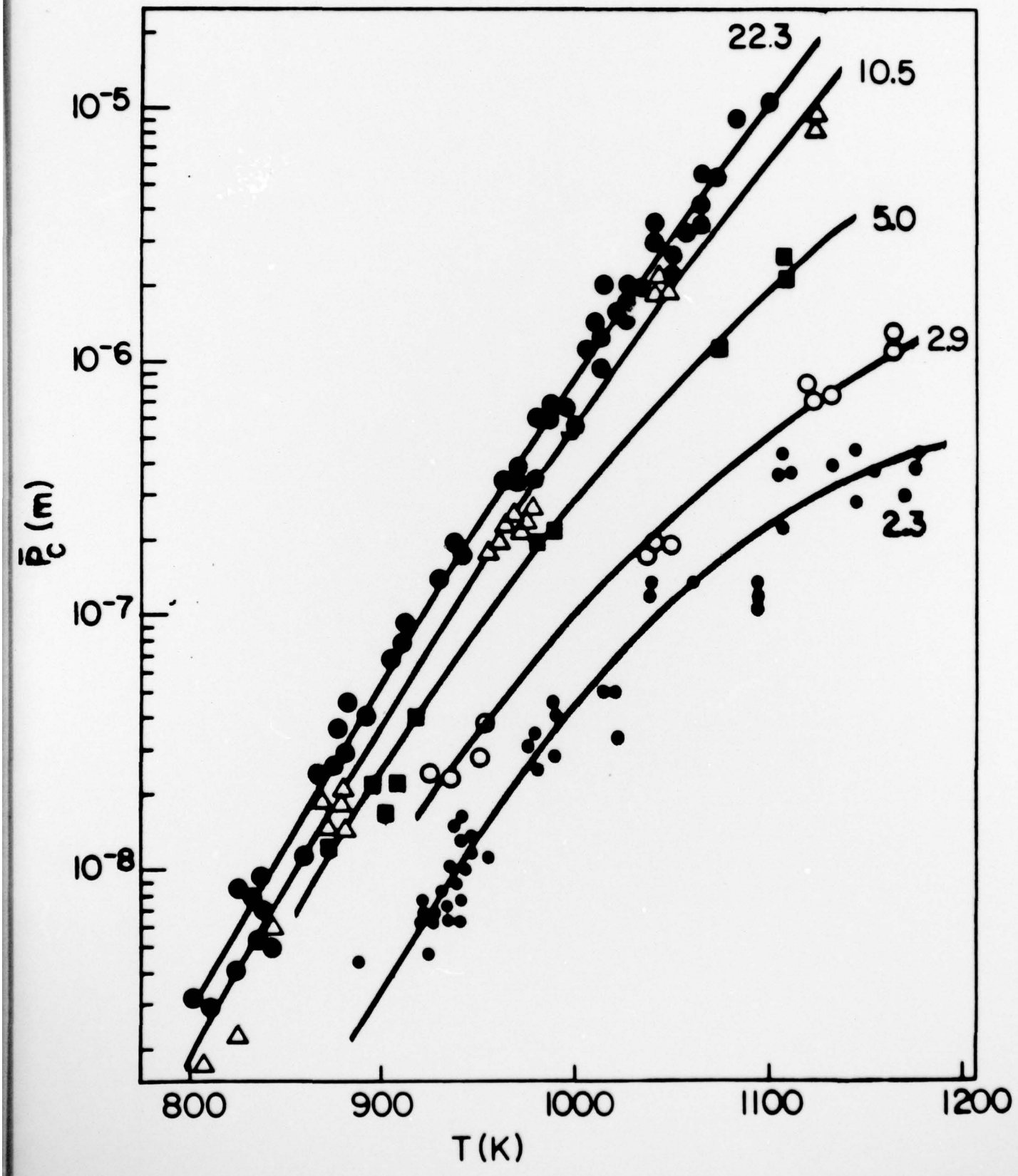
22.3
10.5
5.0
2.9
2.3
10^{-5}
10^{-6}
10^{-7}
10^{-8}
ρ_c (m)
800
900
1000
1100
1200
T(K)

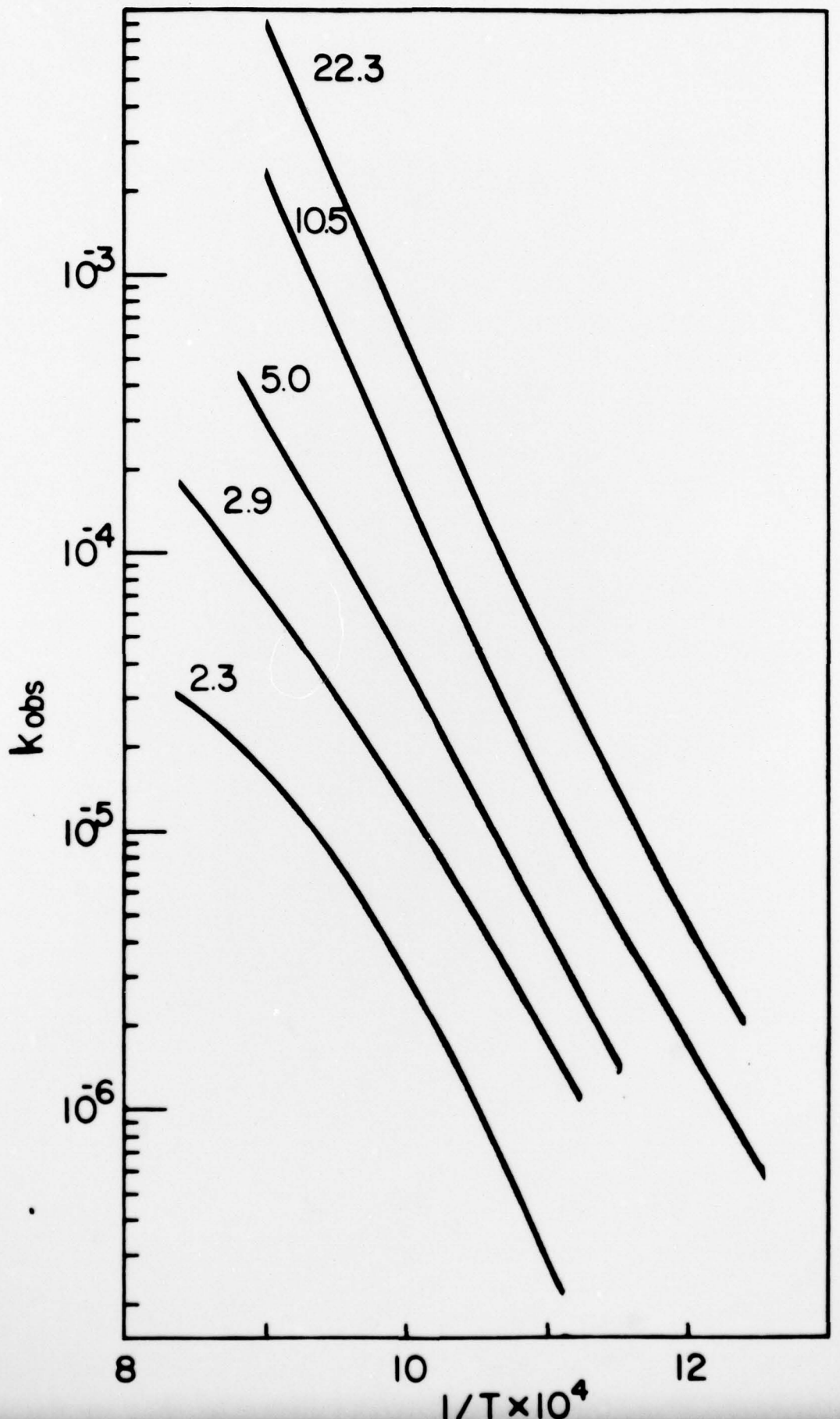
22.3
10.5
5.0
2.9
2.3
10^{-3}
10^{-4}
10^{-5}
10^{-6}
k_{obs}
8
10
12
$1/T \times 10^4$

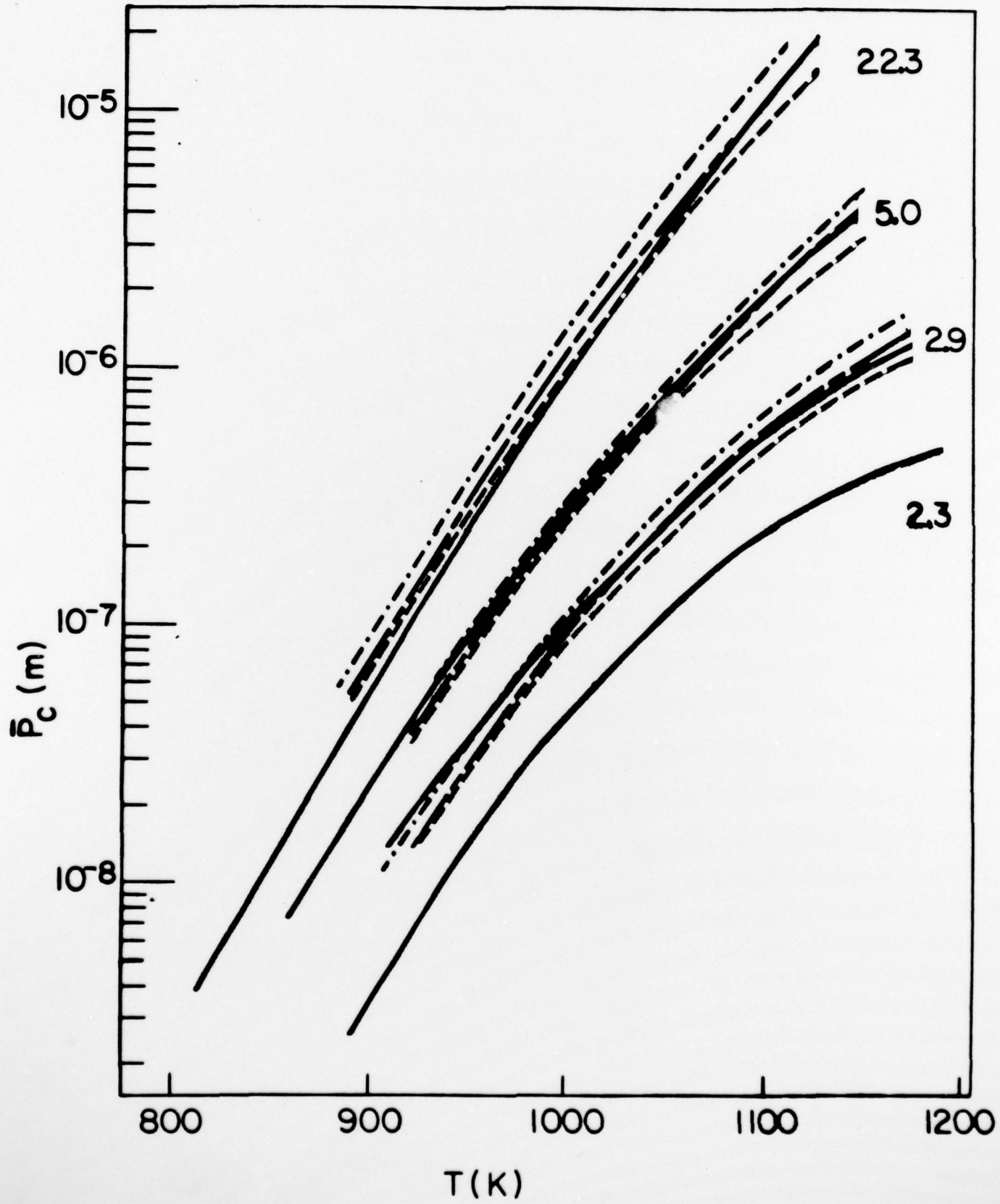

Fig. 3

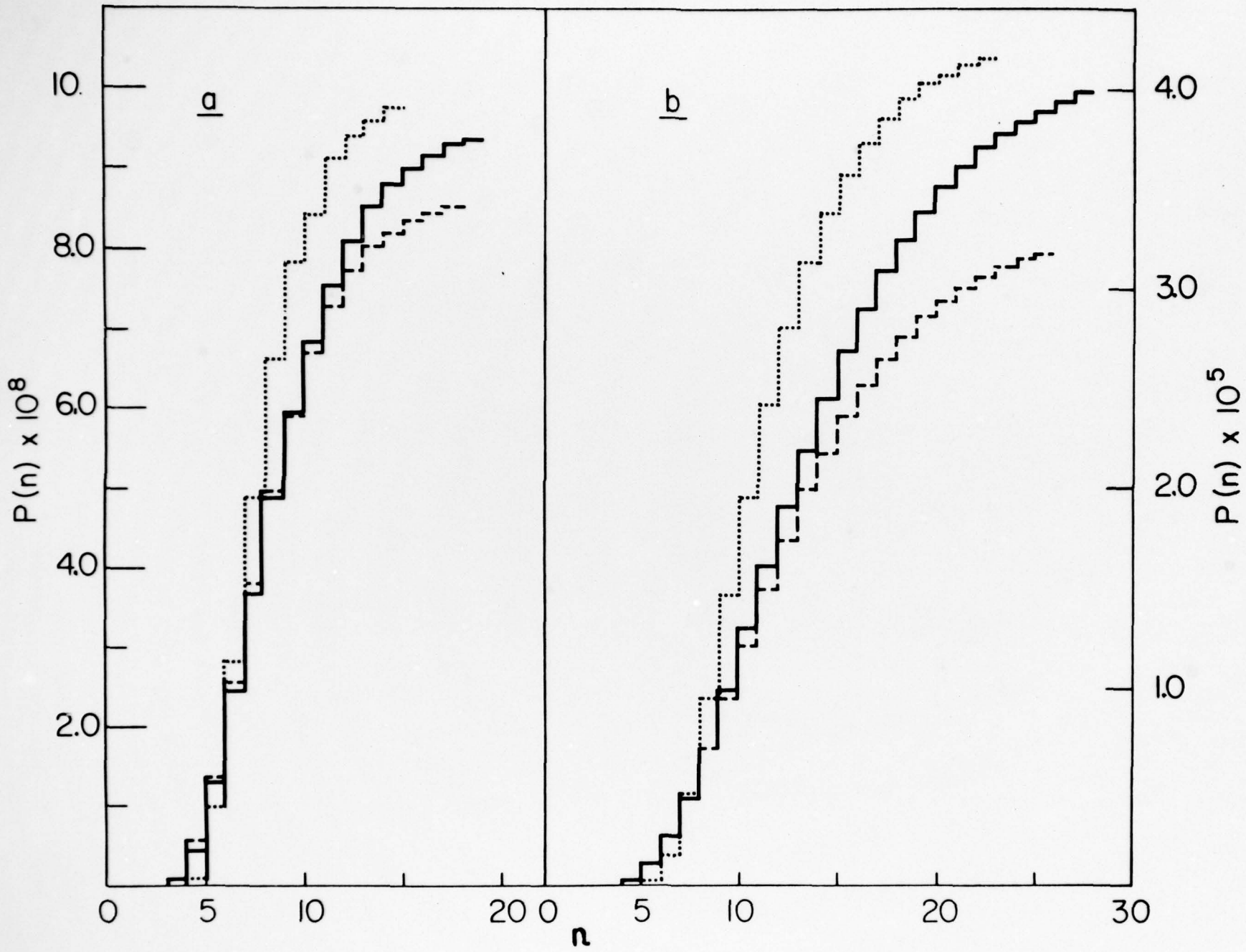

Fig. 4

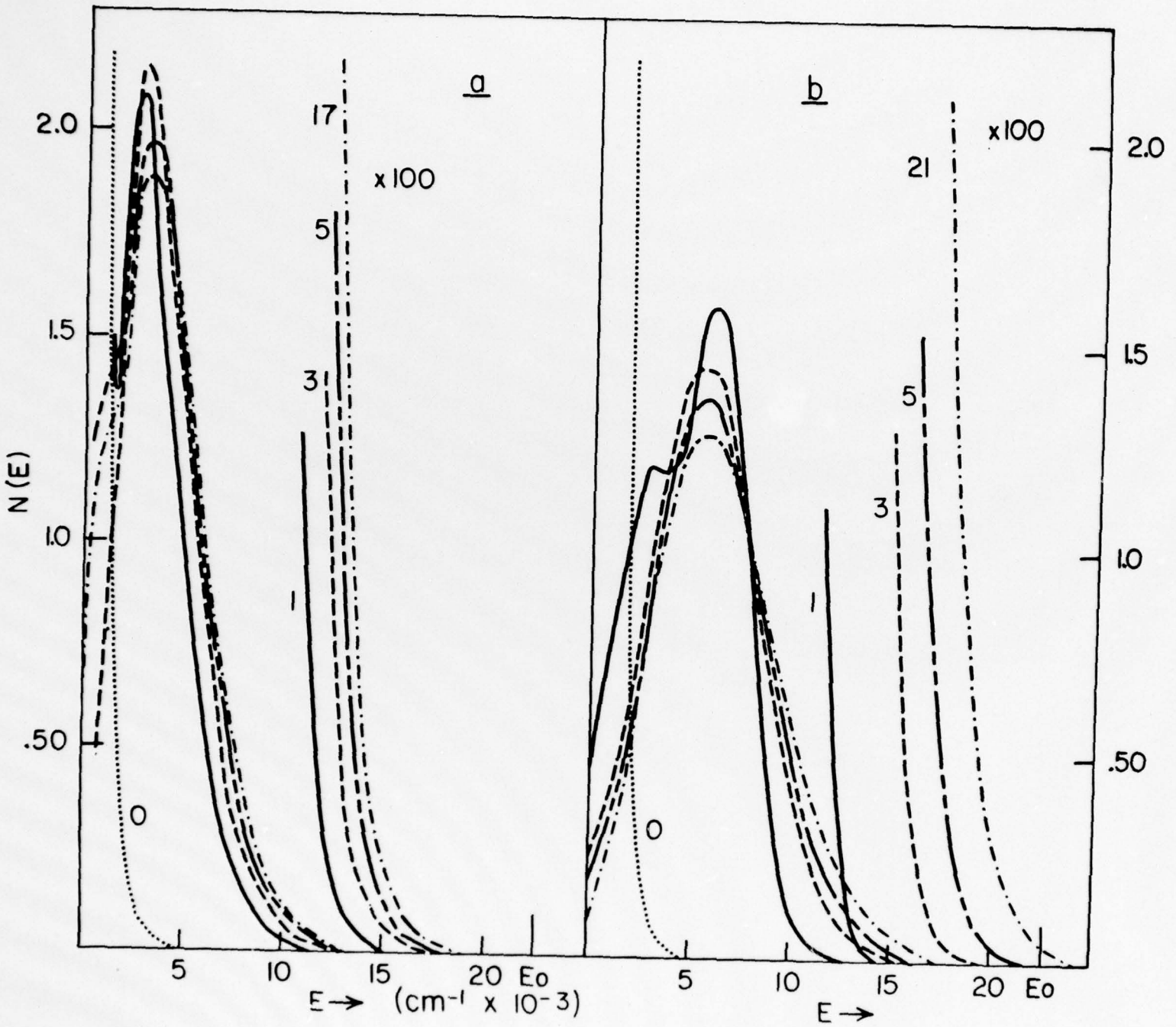
a
b
N(E)
2.0
1.5
1.0
.50
17
x100
5
3
1
0
21
x100
5
3
1
0
5
10
15
20 Eo
E → (cm⁻¹ x 10⁻³)
5
10
15
20 Eo
E →

Fig 5

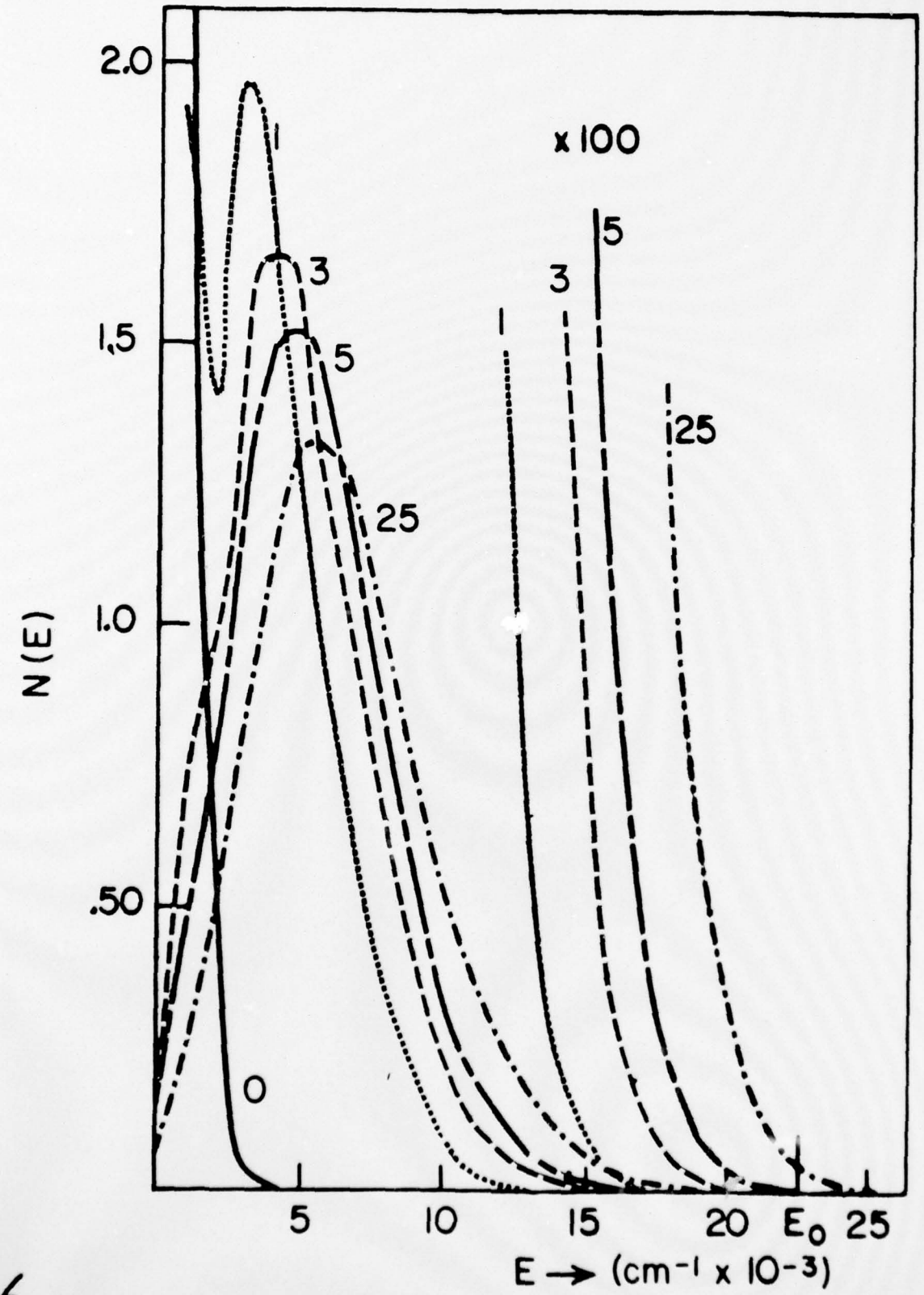

Fig 6

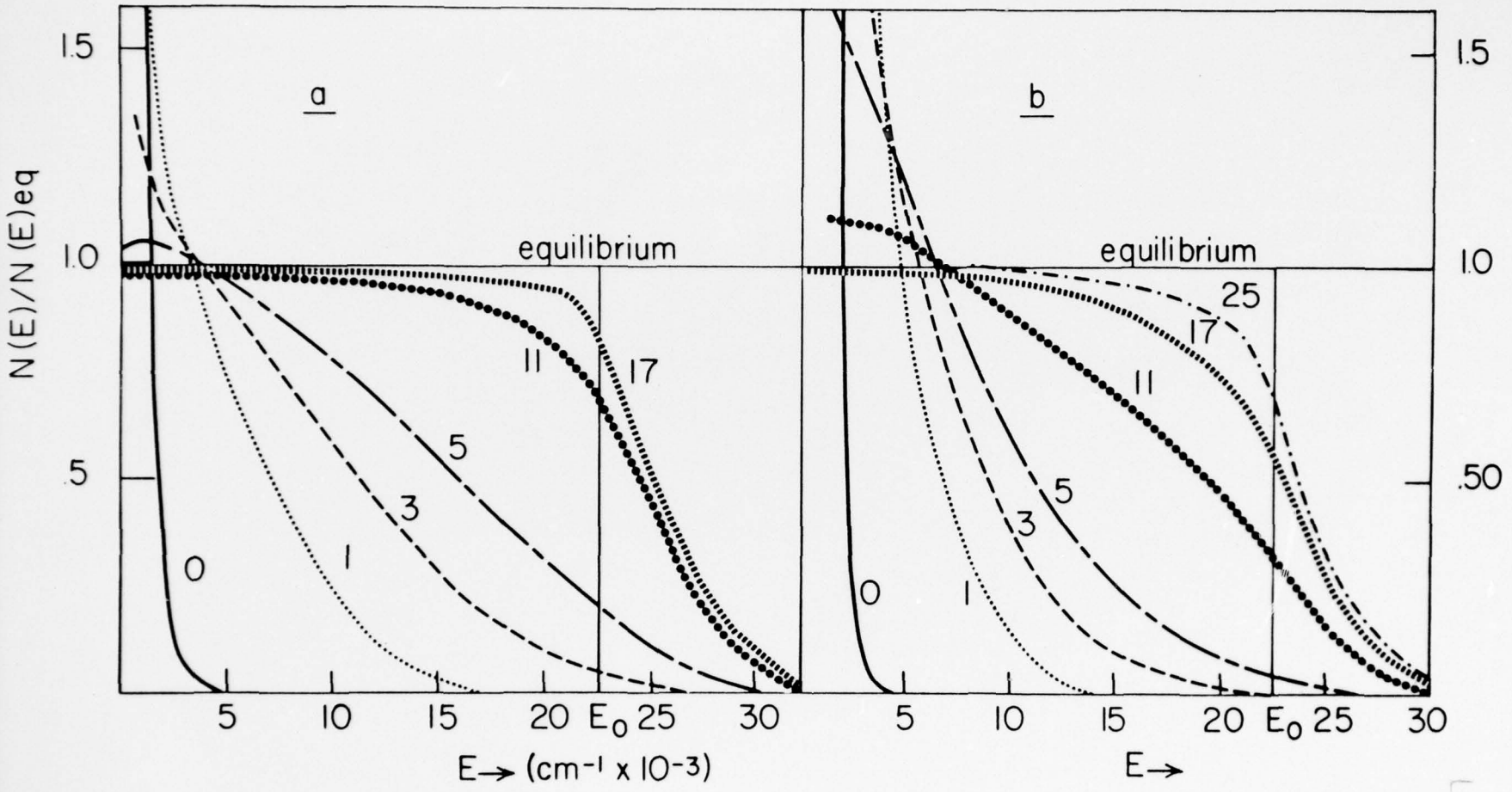
a
b
equilibrium
equilibrium
1.5
1.0
.5
.50
N(E)/N(E)eq
0
1
3
5
11
17
25
5
10
15
20
E_0
25
30
E→ (cm⁻¹ x 10⁻³)
E→

Fig. 1

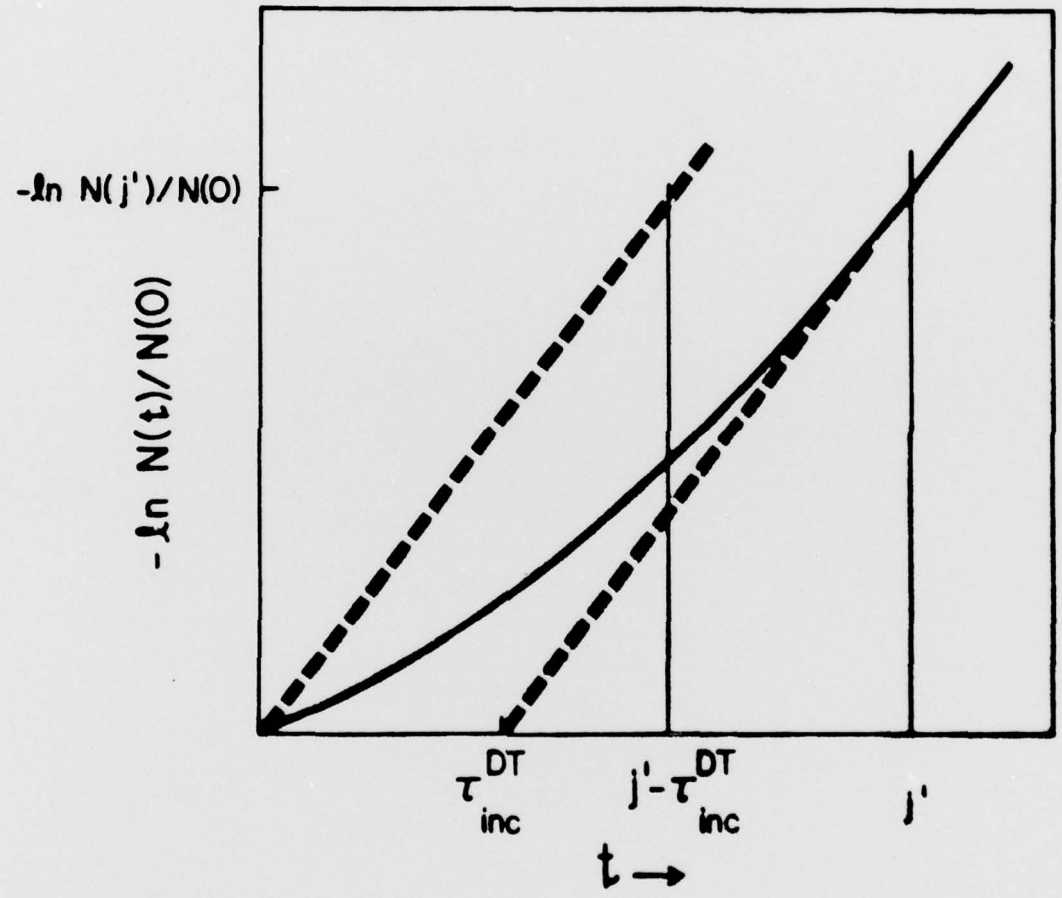

Fig 8